THE JOURNAL OF BIOLOGICAL CHEMISTRY VOL. 286, NO. 51, pp. 44045–44056, December 23, 2011

The Antifungal Drug Itraconazole Inhibits Vascular Endothelial Growth Factor Receptor 2 (VEGFR2) Glycosylation, Trafficking, and Signaling in Endothelial Cells*[S]

Received for publication, July 1, 2011, and in revised form, October 19, 2011 Published, JBC Papers in Press, October 24, 2011, DOI 10.1074/jbc.M111.278754

Benjamin A. Nacev[‡§], **Paola Grassi**[¶], **Anne Dell**[¶], **Stuart M. Haslam**[¶], **and Jun O. Liu**[‡‖1]

From the [‡]*Department of Pharmacology and Molecular Sciences,* [§]*Medical Scientist Training Program, and* [‖]*Department of Oncology, Johns Hopkins University School of Medicine, Baltimore, Maryland 21205 and the* [¶]*Division of Molecular Biosciences, Faculty of Natural Sciences, Imperial College London, London SW7 2AZ, United Kingdom*

Background: Itraconazole is a widely used antifungal drug that was recently found to possess potent antiangiogenic activity.
Results: We report here that itraconazole caused accumulation of immature *N*-glycans on VEGFR2 and inhibited VEGFR2 trafficking and signaling.
Conclusion: These results suggest that itraconazole interferes with VEGFR2 trafficking, glycosylation, and signaling activity.
Significance: Itraconazole possesses unique antiangiogenic potential through targeting multiple pathways that are essential for angiogenesis.

Itraconazole is a safe and widely used antifungal drug that was recently found to possess potent antiangiogenic activity. Currently, there are four active clinical trials evaluating itraconazole as a cancer therapeutic. Tumor growth is dependent on angiogenesis, which is driven by the secretion of growth factors from the tumor itself. We report here that itraconazole significantly inhibited the binding of vascular endothelial growth factor (VEGF) to VEGF receptor 2 (VEGFR2) and that both VEGFR2 and an immediate downstream substrate, phospholipase C γ1, failed to become activated after VEGF stimulation. These effects were due to a defect in VEGFR2 trafficking, leading to a decrease in cell surface expression, and were associated with the accumulation of immature *N*-glycans on VEGFR2. Small molecule inducers of lysosomal cholesterol accumulation and mammalian target of rapamycin (mTOR) inhibition, two previously reported itraconazole activities, failed to recapitulate itraconazole's effects on VEGFR2 glycosylation and signaling. Likewise, glycosylation inhibitors did not alter cholesterol trafficking or inhibit mTOR. Repletion of cellular cholesterol levels, which was known to rescue the effects of itraconazole on mTOR and cholesterol trafficking, was also able to restore VEGFR2 glycosylation and signaling. This suggests that the new effects of itraconazole occur in parallel to those previously reported but are downstream of a common target. We also demonstrated that itraconazole globally reduced poly-*N*-acetyllactosamine and tetra-antennary complex *N*-glycans in endothelial cells and induced hypoglycosylation of the epidermal growth factor receptor in a renal cell carcinoma line, suggesting that itraconazole's effects extend beyond VEGFR2.

Itraconazole is a Food and Drug Administration-approved antifungal drug, which we previously identified as having antiangiogenic activity both *in vitro* and in mouse models (1). Itraconazole's long history of safe use in humans as an antifungal agent and its relatively high plasma concentrations have spurred its advance as a viable candidate for repurposing as an antiangiogenic drug. It is currently undergoing four clinical trials as an anticancer therapeutic (NCT00769600, NCT00887458, NCT00798135, and NCT01108094) and has recently been shown to have efficacy in preclinical models for non-small cell lung cancer (2).

Angiogenesis, the elaboration of new blood vessels from existing vasculature, is an essential process in a number of pathological states, notably cancer and macular degeneration. Since the angiogenic hypothesis was first put forward by Judah Folkman in the 1970s, a number of antiangiogenic drugs have entered the clinic (3). However, these drugs have not been as successful as anticipated. For instance, bevacizumab, an anti-vascular endothelial growth factor (VEGF) antibody and the first to be approved, only marginally extends survival and carries significant risk of adverse events (4–7). For this reason, itraconazole and other drug candidates are being actively pursued as new and potentially more safe and more effective antiangiogenic leads.

Itraconazole, like other members of the azole antifungal class, inhibits the fungal enzyme lanosterol 14-α-demethylase (14DM),[2] which generates a key intermediate in ergosterol syn-

* This work was supported, in whole or in part, by National Institutes of Health (NIH) Medical Scientist Training Program Grant T32GM07309 (to B. A. N.); by NIH, NCI Grant CA122814 (to J. O. L.); National Center for Research Resources (NCRR), NIH, Grant UL1 RR 025005; and the NIH Roadmap for Medical Research. This work was also supported by the Flight Attendant Medical Research Institute and the Commonwealth Foundation (to J. O. L.). Additional support was provided by Biotechnology and Biological Sciences Research Council Grant BBF0083091 and the Marie Curie Initial Training Network, EuroglycoArrays Project, part of the FP7 People Programme.

[S] The on-line version of this article (available at http://www.jbc.org) contains supplemental Fig. 1.

[1] To whom correspondence should be addressed: Jun O. Liu, 725 N. Wolfe St., Hunterian 516, Baltimore, MD 21205. Tel.: 410-955-4619; Fax: 410-955-4620; E-mail: joliu@jhu.edu.

[2] The abbreviations used are: 14DM, lanosterol 14-α-demethylase; HUVEC, human umbilical vein endothelial cell(s); VEGFR2, VEGF receptor 2; PLCγ1, phospholipase C γ1; EGFR, epidermal growth factor receptor; mTOR, mammalian target of rapamycin; RTK, receptor tyrosine kinase; endo H, endoglycosidase H; PNGase F, peptide:*N*-glycosidase F; dMM, deoxymannojirimycin; LacNAc, *N*-acetyllactosamine; ER, endoplasmic reticulum; Sws, swainsonine; PDI, protein disulfide isomerase.

thesis. Conflicting reports on the potency of itraconazole against human 14DM, which is involved in cholesterol synthesis, call into question whether 14DM inhibition is the relevant mechanism for itraconazole's antiangiogenic effects. In addition, we have shown that other azole antifungals are not potent inhibitors of endothelial cell proliferation, an *in vitro* assay for antiangiogenic potential, and that in a complete series of itraconazole stereoisomers, antifungal activity did not track with activity against endothelial cell proliferation (1, 8). This evidence strongly suggests that itraconazole's antiangiogenic properties are elaborated through an as yet unidentified mechanism. Previous attempts to explore itraconazole's cellular effects revealed that in human umbilical vein endothelial cells (HUVEC), itraconazole induces an accumulation of cholesterol in late endsomes/lysosomes and inhibits the mammalian target of rapamycin (mTOR) (9). Itraconazole also inhibits hedgehog signaling in NIH-3T3 cells and in medulloblastoma xenografts and has been shown to inhibit *N*-glycosylation in macrophages (10, 11). How closely these effects are tied to the direct mechanism of itraconazole and to what degree they drive the *in vivo* antiangiogenic effects of the drug is not known.

Angiogenesis is promoted by tumor-elaborated growth factors, such as VEGF and fibroblast growth factor (FGF). These ligands bind to receptor tyrosine kinases (RTKs) expressed on endothelial cells and induce activation of downstream signaling after receptor autophosphorylation. Phospholipase C, phosphatidylinositol-3 kinase, and protein kinase C are among the key signaling intermediates that relay the VEGF binding signal to effectors that ultimately drive endothelial cell proliferation, migration, and survival (12, 13). For both FGF and VEGF, there are multiple RTKs that bind each ligand, and there are multiple isoforms and splice variants of each growth factor. In the case of VEGF-A, the predominant VEGF family member to participate in pathological angiogenesis, there are several RTKs that act as binding partners. These include VEGFR1, VEGFR2, PDGFRα, and PDGFβ as well as the non-RTK co-receptors, neuropilin 1 and 2 (13–15). Of the family of VEGF receptors, VEGFR2 plays the primary role in pathological angiogenesis (12, 16–18).

In our continuing efforts to better understand how itraconazole influences endothelial cell function, we serendipitously observed that treatment of HUVEC with itraconazole significantly altered the migration pattern of VEGFR2 during SDS-PAGE. In this work, we have identified the cause of the migration shift, explored the functional consequences of the itraconazole-induced VEGFR2 changes, and sought to determine the relationship between the previously known activities of itraconazole and the effects we observed on VEGFR2. We have also assessed the degree to which other RTK family members and other cell types were similarly affected by itraconazole.

EXPERIMENTAL PROCEDURES

Chemicals and Reagents—Itraconazole and ketoconazole were purchased from Sigma. Other azoles were obtained from the Johns Hopkins Drug Library (1). Rapamycin and sunitinib were from LC Laboratories. Swainsonine and castanospermine were from Tocris, and deoxymannojirimycin was from Enzo Life Sciences. Recombinant human $VEGF_{165}$ was purchased from R&D systems.

Cell Culture—HUVEC (Lonza) were grown in EGM-2 bullet kit medium (Lonza) and used for experiments at passage eight or lower. ACHN cells (a gift of Prof. Hans Hammers, Johns Hopkins) were grown in minimum Eagle's medium (Invitrogen) supplemented with 10% FBS (Invitrogen) and 1% penicillin/streptomycin (Invitrogen). Both cell lines were maintained in a humidified incubator at 37 °C with 5% CO_2.

Drug Treatment and Western Blotting—Unless otherwise noted, HUVEC were seeded in 6-well dishes at a density of 5×10^4 cells/well in 3 ml of medium and allowed to recover overnight. The medium was then changed to 2 ml of fresh medium, and drugs were immediately added from 200× DMSO (Fisher) stocks along with vehicle controls. In experiments with ACHN cells, cells were seeded at a density of 2×10^5 cells/well. After a 24-h treatment, the cells were lysed by the addition of SDS sample buffer and incubated on ice for 10 min followed by boiling for 10 min. For phospho-VEGFR2 (Cell Signaling, catalog no. 2478), VEGFR2 (Cell Signaling, catalog no. 2479), VEGFR1 (Cell Signaling, catalog no. 2893), PLCγ1 (Cell Signaling, catalog no. 2822), and phospho-PLCγ1 (Cell Signaling, catalog no. 2821) blotting, lysates were subjected to 6 or 8% SDS-PAGE. For pS6K (Cell Signaling, catalog no. 9205), S6K (Santa Cruz Biotechnology, Inc., catalog no. sc-8418), phospho-ERK1/2 (Cell Signaling, catalog no. 9101), ERK1/2 (Santa Cruz Biotechnologies, Inc., catalog no. sc-94), and epidermal growth factor receptor (EGFR) (Cell Signaling, catalog no. 2232) blotting, proteins were separated by 10% SDS-PAGE. Proteins were transferred to PVDF (Bio-Rad) or nitrocellulose (Bio-Rad) in the case of phospho-S6K blots. Membranes were blocked with 5% bovine serum albumin (BSA) (Sigma) in TBS-T (0.5% Tween 20 (Sigma)) and then incubated with primary antibody in 1% BSA in TBS-T, followed by incubation with HRP-conjugated anti-rabbit or anti-mouse IgG (GE Healthcare) also in 1% BSA in TBS-T. In the case of phospho-S6K blots, blocking and all incubation steps were carried out in 5% blotto (Santa Cruz Biotechnology, Inc.) in TBS-T. Membranes were washed three times with TBS-T before and after the secondary antibody incubations. HRP substrate (Immobilon Western, Milipore) was added for 1–5 min, and bands were visualized with an Eastman Kodak Co. Image Station 440 CF. Quantitation of band intensity was carried out with ImageJ using the background subtraction module (version 1.43u, National Institutes of Health). All Western blots shown are representative of three independent experiments with the exception of the ^{125}I-$VEGF_{165}$ experiments, which were performed in duplicate.

VEGF Stimulation Experiments—1.5×10^5 HUVEC in 4 ml of medium were seeded in a 6-cm dish and allowed to recover overnight. The medium was then changed to 2 ml of basal EGM-2 medium with 0.1% FBS, and cells were treated with drugs from 200× DMSO stocks or vehicle alone for 24 h. Recombinant human $VEGF_{165}$ was then added to a final concentration of 25 ng/ml from a 100× stock in basal EGM-2 with 0.1% FBS freshly prepared from frozen 100 μg/ml stocks in 0.1% BSA in PBS. The cells were stimulated for 2–60 min and transferred to ice along with an unstimulated control. The medium was aspirated, and the cells were immediately lysed with the addition of 240 μl of 2× SDS sample buffer. After a 10-min

incubation on ice, the lysates were boiled for 10 min and then subjected to SDS-PAGE.

Filipin Staining—These experiments were based on previous work (9). HUVEC were seeded at 3×10^4 cells/well of an 8-chamber glass slide (Lab-Tek) in 400 μl of medium. After an overnight recovery, drugs were added from 200× DMSO stocks along with vehicle controls. Following a 24-h treatment, the cells were fixed in 4% paraformaldehyde in PBS (pH 7.4) for 20 min and then washed three times with 400 μl of PBS. 200 μl of filipin staining solution (50 μg/ml filipin (Sigma, catalog no. F9765) diluted from a 100× stock in DSMO stored in the dark and made from powder stored under argon) and slides were incubated in the dark for 2 h at room temperature. The cells were then washed three times with 400 μl of PBS, mounted with Immu-mount (Thermo), and stored in the dark prior to imaging with a Zeiss AxioExaminer with 710NLO-Meta multiphoton and confocal module. These experiments were performed in duplicate.

Proliferation Assays—These assays were performed as reported previously (19). ACHN cells were seeded at 8,000 cells/well.

^{125}I-VEGF Receptor Cross-linking—These experiments were adapted from the methods of Neufeld and co-workers (20, 21). 3×10^5 HUVEC were seeded on 6-cm dishes in 4 ml of medium and allowed to recover overnight. The medium was changed to 2 ml of basal EGM-2 with 0.1% FBS, and either vehicle or itraconazole (800 nM final concentration) from a 200× DSMO stock was added. After a 24-h incubation, the plate was transferred to 4 °C and washed twice with 5 ml of ice-cold PBS. An aliquot of 1.4 ml of serum-free EGM-2 with 5 ng/ml ^{125}I-$VEGF_{165}$ (PerkinElmer Life Sciences) (diluted from a 100× stock) was added. For one of two vehicle-treated plates, 100 ng/ml cold $VEGF_{165}$ was also added to the medium prior to transfer to the cells (competition sample). The cold $VEGF_{165}$ was diluted from a 100 μg/ml stock in 0.1% BSA in PBS. After a 2-h incubation with rocking at 4 °C, the cells were washed once with 4.5 ml of ice-cold PBS and moved to room temperature. An aliquot of 2.5 ml of 0.15 mM disuccinimidyl suberate (Sigma) in PBS (diluted from a freshly made 20 mM stock in DMSO) was added, and the incubation was continued for 15 min prior to the addition of 200 μl of quenching buffer (10 mM Tris-HCl (pH 7.5), 200 mM glycine, 2 mM EDTA). After a 1-min incubation, the plates were returned to 4 °C and washed once with 4.5 ml of PBS. An aliquot of 200 μl of ice-cold lysis buffer (50 mM Tris-HCl (pH 7.5), 150 mM NaCl, 1% Nonidet P-40, 10 mM EDTA, 10% glycerol, protease inhibitors (Complete EDTA-free; Roche Applied Science)) was then added, and the cells were scraped from the plates and collected in a 1.5-ml tube, which was then rested at 4 °C for 15 min. The tubes were then spun at 10,000 × *g* at 4 °C for 10 min, and the supernatant was transferred to a new tube. An aliquot of 200 μl of the supernatant was combined in a 0.5-ml tube with 1.5 μg of anti-VEGR2 antibody (Cell Signaling, catalog no. 2479) from a 1 mg/ml stock in PBS and incubated for 2 h at 4 °C on a rotating wheel. The mixture was then added to 30 μl of protein A Dynabeads (Invitrogen), which were prewashed with 1 ml of PBS in a 0.5-ml tube and rotated for 20 min at 4 °C, after which time the mixture was transferred to a 1.5-ml tube and washed three times with 500 μl of 0.1% Nonidet P-40 in PBS. The beads were then resuspended in 100 μl of PBS and transferred to a new tube. The supernatant was removed, and the beads were boiled in 90 μl of 1× SDS sample buffer. The samples were split into two equal volumes, and the proteins were subjected to 6% SDS-PAGE. One set of samples was transferred to a PVDF membrane, and VEGFR2 was analyzed by Western blot. The other was fixed in the gel by incubation with 10% acetic acid and 30% MeOH for 0.5 h and then dried for 2 h at 80 °C. The dried gel was exposed to film for 3–4 weeks at −70 °C prior to developing.

Global N-Glycan Analysis—9.2×10^5 HUVEC were seeded in 15-cm dishes and allowed to recover overnight in 20 ml of medium. The medium was then changed to 36.5 ml of fresh medium, and the cells were treated with 800 nM itraconazole (from a 200× DMSO stock) or vehicle alone for 24 h. The plates were washed three times with 15 ml of ice-cold PBS and then scraped into 5 ml of ice-cold PBS, collected by centrifugation (500 × *g*), and frozen in liquid N_2. Approximately 9×10^6 cells from each treatment condition were processed as described previously (22, 23). Briefly, all samples were subjected to homogenization using a 130-watt Vibra-Cell ultrasonic processor (VC 130 PB, Sonics & Materials) within a sound-abating enclosure in extraction buffer (25 mM Tris, 150 mM NaCl, 5 mM EDTA, and 1% CHAPS at pH 7.4) and subsequently dialyzed against 4 × 4.5 liters of 50 mM ammonium bicarbonate, pH 8.5, at 4 °C for 48 h.

After dialysis, the samples were lyophilized and subjected to reduction, carboxymethylation, and tryptic digestion. Reduction was carried out in 1 ml of 50 mM Tris-HCl buffer, pH 8.5, containing 2 mg/ml dithiothreitol, at 37 °C in a water bath for 1 h. The samples were then carboxymethylated by the addition of iodoacetic acid (5-fold molar excess over dithiothreitol), and the reaction was allowed to proceed at room temperature in the dark for 1.5 h. Carboxymethylation was terminated by dialysis against 4 × 4.5 liters of 50 mm ammonium bicarbonate, pH 8.5, at 4 °C for 48 h. After dialysis, the samples were lyophilized. The reduced carboxymethylated proteins were then digested with *N-p*-tosyl-L-phenylalanine chloromethyl ketone-pretreated bovine pancreas trypsin (EC 3.4.21.4; Sigma) for 16 h at 37 °C in 50 mM ammonium bicarbonate buffer, pH 8.4. The products were purified by C18 Sep-Pak® (Waters) as described previously (24).

Peptide *N*-glycosidase F digestion of the tryptic glycopeptides was carried out in 50 mM ammonium bicarbonate buffer, pH 8.5, for 20 h at 37 °C with 5 units of enzyme (Roche Applied Science). The released *N*-glycans were purified from *O*-glycopeptides and peptides by chromatography on a Sep-Pak C18 cartridge (Waters Corp., Milford, MA) and subsequently methylated using the sodium hydroxide permethylation procedure as described previously (22).

MALDI-TOF data were acquired on a Voyager-DE STR mass spectrometer (Applied Biosystems, Foster City, CA) in the reflectron mode with delayed extraction. Permethylated samples were dissolved in 10 μl of 70% (v/v) aqueous methanol, and 1 μl of the dissolved sample was premixed with 1 μl of matrix (20 mg/ml 2,5-dihydroxybenzoic acid in 70% (v/v) aqueous methanol), spotted onto a target plate, and dried under vacuum.

The MS data were processed using Data Explorer 4.9 software (Applied Biosystems). The mass spectra were base line-corrected (default settings) and noise-filtered (with a correction factor of 0.7) and then converted to ASCII format. The processed spectra were then subjected to manual assignment and annotation with the aid of the glycobioinformatics tool GlycoWorkBench (25).

N-Glycan Digestions—HUVEC were seeded at 4×10^5 cells/10 ml of medium in a 10-cm dish. After an overnight recovery, the medium was changed to 8 ml of fresh medium, and the cells were treated with itraconazole from a 200× stock in DMSO or vehicle alone. The cells were washed twice with 10 ml of ice-cold PBS and lysed by the addition of 500 μl of lysis buffer (50 mM Tris (pH 7.5), 150 mM NaCl, 1 mM EDTA, 1% Triton-X-100, protease inhibitors (Complete EDTA-free, Roche Applied Science)) with rocking at 4 °C for 20 min. The lysates were collected by scraping the dish and then centrifuged for 10 min, 10,000 × *g* at 4 °C. The protein concentration in the supernatant was measured using a D_c protein assay kit (Bio-Rad) and normalized by the addition of lysis buffer as needed. Equal amounts of protein (19–34 μg) were digested at 37 °C in 300-μl reactions with sialidase (specificity for α2–3, α2–6, and α2–8 *N*-acetyl-neuraminic acid residues), endo H, and PNGase F purchased from New England Biolabs according to the manufacturer's instructions. The sialidase reaction was carried out for 5 min, and the endo H and PNGase F reactions were carried out for 40 min. At the end of the reaction, the samples, along with undigested controls, were boiled in SDS sample buffer and analyzed by Western blot. In the case of ACHN cells, the procedure was modified as follows. 1.5×10^6 cells were seeded on 10-cm dishes in 10 ml of medium with 10% FBS and allowed to recover overnight. The medium was changed to 10 ml of fresh medium with 2% serum, and the cells were treated with drugs for 24 h. A sample of 100 μg of protein was used for each digestion.

Surface Protein Biotinylation—HUVEC were seeded and treated with drugs as in the VEGF binding experiments, except that the drug incubations were done in 4 ml of medium. Following the treatment period, the cells were washed twice with 5 ml of ice-cold PBS and then incubated with 2.5 ml of ice-cold 0.5 mg/ml Sulfo-NHS-LC-Biotin (Thermo) in PBS for 30 min with rocking at 4 °C. After washing once with 5 ml of ice-cold PBS, the cells were incubated with 2.5 ml of 25 mM Tris (pH 8.0) for 15 min at 4 °C. The cells were again washed with 5 ml of ice-cold PBS and then lysed in 200 μl of lysis buffer (50 mM Tris (pH 8.0), 150 mM NaCl, 0.1% SDS, 1% Nonidet P-40, 0.5% sodium deoxycholate, 10 mM pyrophosphate, 10 mM glycerophosphate, 50 mM NaF, 0.5 mM $NaVO_4$, protease inhibitors (Complete EDTA-free, Roche)) by incubation for 20 min at 4 °C. The lysates were collected by scraping the dish and then centrifuged for 10 min, 10,000 × *g* at 4 °C. The protein concentration in the supernatant was determined using a D_c protein assay kit (Bio-Rad) and normalized by the addition of lysis buffer as needed. An aliquot of 200 μl of supernatant was then applied to high capacity steptavidin-agarose beads (Thermo), which had been equilibrated with two 5-min incubations with 1 ml of lysis buffer. A sample of lysate was also boiled for 10 min in SDS sample buffer as an input control. After a 1-h incubation with rotation at 4 °C, the beads were washed three times in 1 ml of lysis buffer (5 min of rotation per wash) and subsequently boiled in 60 μl of 2× SDS sample buffer for 10 min. The supernatant was then run on SDS-PAGE along with the input fractions and analyzed by Western blot.

Sterol Rescue Experiments—These experiments were based on work by Christian *et al.* (26) that was previously applied to the rescue of itraconazole-induced effects in HUVEC (9). HUVEC were seeded at 5×10^4 cells/well in a 6-well dish in 3 ml of medium. After an overnight recovery, the medium was changed to 2 ml of fresh medium, and the free sterols, free methyl-β-cyclodextrin, and sterol·methyl-β-cyclodextrin complexes were added from 100× stocks followed by drug addition from 200× stocks in DMSO or vehicle alone. To prepare the sterol·methyl-β-cyclodextrin complexes, cholesterol (Sigma) or β-estradiol (Sigma) from 20 mg/ml stocks in ethanol were combined with filter-sterilized 10% methyl-β-cyclodextrin (Sigma) in PBS to give a final 0.4 mg/ml sterol concentration. Aliquots of 0.4 mg/ml sterol in PBS only, 10% methyl-β-cyclodextrin with ethanol vehicle, and ethanol in PBS only were also prepared. All samples were solubilized by three cycles of vortexing followed by ~5-min incubations at 42 °C prior to the addition to cells to give 4 μg/ml sterol and 0.1% methyl-β-cyclodextrin final concentrations. All solutions were prepared fresh. At the end of a 24-h incubation, the samples were processed for Western blotting as described above.

Immunofluorescence—HUVEC were seeded at 2×10^4 cells/well of a 12-well dish in 1 ml of medium on an EtOH-sterilized 18-mm glass coverslip (Fisher). After an overnight recovery, the medium was changed to 1 ml of fresh medium, and the cells were treated with drugs from 200× stocks in DMSO or vehicle alone for 24 h. The medium was then aspirated, and the cells were fixed in 0.7 ml of 4% paraformaldehyde in PBS for 20 min. Following three washes with 0.7 ml of PBS, the cells were permiabilized with 0.7 ml of 0.1% Triton X-100 in PBS for 2 min and then blocked with 0.7 ml of 2% filtered goat serum (Sigma) in PBS for 1 h at room temperature. The blocking solution was removed, and the coverslips were incubated overnight at 4 °C with 25 μl of primary antibody solution (1:50 anti-VEGFR2 (Cell Signaling, catalog no. 2479) and 1:50 anti-PDI (Enzo, catalog no. ADI-SPA-891) or 1:1000 anti-GM130 (BD Biosciences, catalog no. 610823) in 1.25% BSA in PBS). The coverslips were then washed three times in 0.7 ml of PBS and incubated for 1 h at room temperature with 25 μl of secondary antibody solution (1:800 goat anti-rabbit Alexafluor 488 (Invitrogen, catalog no. A11008), 1:800 goat anti-mouse Alexafluor 594 (Invitrogen, catalog no. A11005), and DAPI (0.1 μg/ml) in 1.25% BSA in PBS). Following three washes with 0.7 ml of PBS, the coverslips were mounted with 15 μl of Immumount (Fisher) and sealed with clear nail polish. Confocal imaging was performed using a Zeiss 710NLO Meta multiphoton confocal microscope and Zen software (Carl Zeiss). Representative micrographs were taken of 2 fields/condition/independent experiment.

RESULTS

Itraconazole Induces the Accumulation of a Low Apparent Molecular Weight VEGFR2 Species—VEGFR2 ordinarily exists as a major high molecular weight species and a minor lower

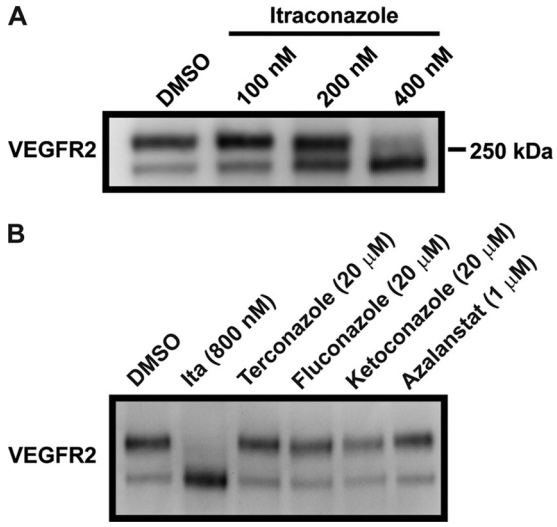

FIGURE 1. **Itraconazole induces a change in the migration pattern of VEGFR2.** *A*, HUVEC were treated for 24 h with the indicated doses of itraconazole or vehicle (DMSO), and VEGFR2 was analyzed by Western blot. *B*, HUVEC were treated as in *A* with three inhibitors of fungal 14DM (terconazole, fluconazole, and ketoconazole) and an inhibitor of human 14DM (azalanstat).

molecular weight species as seen on SDS-PAGE. We observed that in HUVEC treated with itraconazole, the migration pattern of VEGFR2 was altered such that only the lower molecular weight species was present (Fig. 1*A*). The shift from the high to low molecular weight species was apparent when HUVEC were treated with 200 nM itraconazole and was nearly complete at 400 nM itraconazole, which is in line with the IC_{50} we have previously reported for the itraconazole-induced inhibition of HUVEC proliferation, cholesterol accumulation, and mTOR inhibition (1, 9). The correlation of these potencies suggested to us that the effects were related to a similar underlying mechanism and therefore warranted further exploration.

Because itraconazole inhibits 14DM, we first tested whether this activity contributed to the VEGFR2 migration pattern shift. We treated HUVEC with terconazole, fluconazole, and ketoconazole, which are three other members of the azole antifungal class, and azalanstat, a non-azole small molecule inhibitor of human 14DM with an apparent K_i of 800 pM (27). None were able to induce similar changes in VEGFR2 migration (Fig. 1*B*). Notably, ketoconazole has significant crossover inhibition of human 14DM at doses much lower than we used here (28, 29). Thus, 14DM inhibition could not explain the effects of itraconazole on VEGFR2.

Itraconazole Prevents VEGF-stimulated Signaling by VEGFR2—Having observed the itraconazole-induced changes in VEGFR2 migration, we hypothesized that VEGFR2 function may be perturbed. To test this, HUVEC were incubated in reduced serum medium in the presence of varying does of itraconazole or vehicle and then stimulated with $VEGF_{165}$ for 2–60 min alongside unstimulated controls. After stimulation, the cells were immediately lysed, and the ligand-induced autotransphosphorylation of the receptor at Tyr-1175, a requirement for VEGFR2 signaling, was determined by Western blotting (30). Phosphorylation of phospholipase C γ1 (PLCγ1), a direct binding partner of VEGFR2 that signals downstream in a phospho-Tyr-1175-dependent manner, was also examined (30–32) (Fig. 2*A*). In vehicle-treated cells, VEGFR2 and PLCγ1 phosphorylation peaked by 2 min after VEGF addition, and the signal decayed by 30 min after stimulation. In HUVEC treated with 400 nM itraconazole, VEGFR2 phosphorylation was inhibited by 80% ($p < 0.05$), and PLCγ1 phosphorylation was inhibited by 60% ($p < 0.05$) at 2 min after VEGF stimulation (Fig. 2, *A* and *B*). There was no increase in phosphorylation with time, suggesting that the decrease in phosphorylation at 2 min was not simply a result of itraconazole delaying the kinetics of receptor activation. Treatment with 800 nM itraconazole slightly increased the inhibition of PLCγ1 phosphorylation compared with the 400 nM dose but did not further suppress VEGFR2 phosphorylation, which was already near the limit of detection by Western blot. Notably, the degree of VEGFR2 phosphorylation inhibition by 400 nM itraconazole was similar to that observed by treatment with sunitinib, an antiangiogenesis drug that has efficacy against renal cell carcinoma, gastrointestinal stromal tumors, and pancreatic neuroendocrine tumors and directly inhibits VEGFR2 kinase activity (33, 34). Interestingly, although sunitinib strongly inhibited the phosphorylation of ERK1/2, a downstream effector of the VEGFR2 signaling, itraconazole at doses up to 800 nM did not block ERK1/2 activation after VEGF addition.

In order for VEGFR2 to become activated, the receptor must first bind VEGF, dimerize, and then undergo autophosphorylation in *trans* (18, 35). Given the strong inhibition of VEGF-stimulated VEGFR2 signaling by itraconazole, we next sought to determine which step of VEGFR2 activation was perturbed. Following the techniques used by Neufeld and co-workers (20, 21) to initially identify the VEGFR2 receptor on the basis of VEGF binding, we evaluated the ability of VEGFR2 in itraconazole-treated cells to bind ^{125}I-$VEGF_{165}$. After drug treatment using the same conditions as in the signaling experiments, HUVEC were stimulated with the radiolabeled ligand, which was then cross-linked to the receptor with the bidentate cross-linking agent disuccinimidyl suberate. Because VEGF binds a number of receptors but we were specifically interested in VEGFR2, we immunoprecipitated VEGFR2 and evaluated the resultant fraction by Western blot and autoradiography (Fig. 2*C*). As expected, there was strong labeling of VEGFR2 after vehicle treatment, which was abrogated by the addition of a 20-fold excess of cold $VEGF_{165}$ during the ligand-binding step. In contrast, itraconazole treatment resulted in a nearly complete loss of labeling, suggesting that itraconazole prevented VEGF binding to VEGFR2.

Complete N-Glycosylation of VEGFR2 Is Inhibited by Itraconazole—Given the clear inhibition of VEGFR2 signaling and ligand binding after itraconazole treatment, we next focused on understanding the nature of the itraconazole-induced VEGFR2 molecular weight changes. Because itraconazole was recently shown to interfere with the glycosylation of the CD14 receptor and other proteins in macrophages, we had a strong suspicion that itraconazole was also modulating VEGFR2 glycosylation, thereby leading to the altered migration of the protein (11). This model is consistent with early work on VEGFR2, which revealed that the protein was *N*-glycosylated and that in [^{35}S]methionine pulse-chase experiments, the newly synthesized protein transits through a low molecular

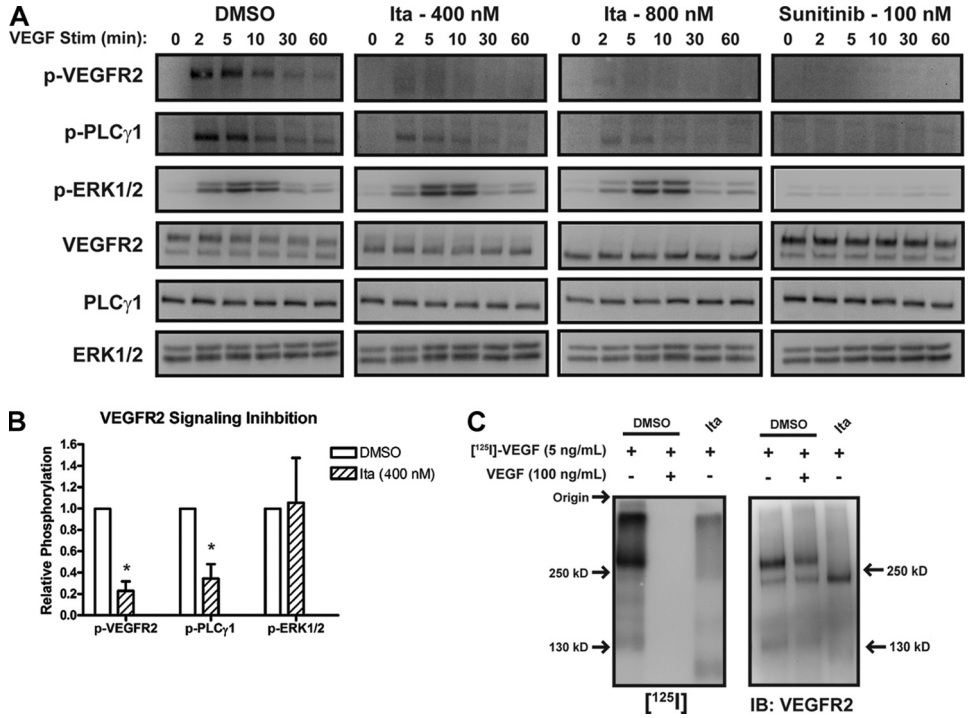

FIGURE 2. **Itraconazole blocks $VEGF_{165}$ binding to VEGFR2 and inhibits VEGFR2 signaling.** *A*, HUVEC were grown in low serum medium for 24 h in the presence of vehicle (DMSO), itraconazole (*Ita*), or the VEGFR2 inhibitor sunitinib. The cells were then stimulated for the indicated times with $VEGF_{165}$, lysed, and analyzed by Western blot for an activating phosphorylation on VEGFR2 (Tyr-1175), its immediate downstream binding partner PLCγ1 (Tyr-783), and a downstream effector ERK1/2 (Thr-202/Tyr-204). Total protein levels are shown as controls. *B*, for the 400 nM itraconazole samples, the phosphorylated signals were quantitated, normalized to the levels of total protein and then to vehicle control. $n = 3$ independent experiments; *error bars*, S.E.; *, $p < 0.05$. *C*, HUVEC were treated with 800 nM itraconazole or vehicle under the same conditions as in *A* and then were incubated with ^{125}I-$VEGF_{165}$ with or without competition with cold $VEGF_{165}$ (20-fold excess). The ligand was cross-linked to VEGFR2, which was then immunoprecipitated and subject to both autoradiography and Western blotting (*IB*) for VEGFR2.

weight intermediate similar in size to the species that accumulates after itraconazole treatment (31). The same study also showed that only the mature protein contained phosphorylated tyrosines after VEGF stimulation, which is similar to our observations on the itraconazole-induced changes in VEGFR2.

We thus examined the effects of various known inhibitors of *N*-linked glycosylation on VEGFR2 and compared them with that of itraconazole. Altering glycosylation in HUVEC using tunicamycin, swainsonine, deoxymannojirimycin (dMM), or castanospermine, inhibitors of different enzymes in the N-glycosylation pathway, clearly affected the migration pattern of VEGFR2 (Fig. 3, *A* and *C*). This suggested that perturbed glycosylation in HUVEC might underlie the mobility shifts seen after itraconazole treatment. Interestingly, time course experiments with tunicamycin and dMM indicated that they induced VEGFR2 shifts much more rapidly than itraconazole (Fig. 3, *B* and *C*). We next digested lysates from itraconazole or vehicle-treated HUVEC with sialidase, which cleaves α2–3, α2–6, and α2–8 *N*-acetyl-neuraminic acid residues from complex *N*-glycans; endo H, which releases either hybrid or oligomannose *N*-linked sugars; and PNGase F, which releases all *N*-linked sugars, respectively (Fig. 3*D*). Western blots of vehicle-treated lysates showed that the upper band was sensitive to sialidase and PNGase F, whereas the lower band was sensitive to endo H and PNGase F. This confirms that both species are *N*-glycosylated and indicates that the upper band contains the more highly processed complex *N*-glycans. In contrast, all of the VEGFR2 present in the lysates from itraconazole-treated cells was sensitive to both endo H and PNGase F but was insensitive to sialidase. This indicated that the VEGFR2 migration shift observed after itraconazole treatment was due to the accumulation of a hypoglycosylated VEGFR2 species.

Because the ER contains the calnexin/calreticulin quality control chaperones that retain improperly glycosylated proteins, we performed cell surface biotinylation experiments to determine if trafficking of the hypoglycosylated VEGFR2 was disturbed (36). After treatment under the same conditions in which we assessed VEGFR2 signaling and VEGF binding, cell surface proteins were reacted with NHS-biotin and then captured on streptavidin beads after lysis (pull-down fraction) and analyzed by Western blot. In contrast to tubulin, which is an intracellular protein and therefore not biotinylated, VEGFR2 from vehicle-treated cells was present in the pull-down fraction (Fig. 3*F*). However, itraconazole treatment strongly reduced the levels of VEGFR2 on the cell surface.

To determine the fate of the hypoglycosylated VEGFR2, its subcellular localization was determined by immunofluorescence (Fig. 4*A*). In itraconazole-treated cells, VEGFR2 accumulated in a unipolar, perinuclear, Golgi-like structure, which partially colocalized with the *cis*-Golgi marker, GM130. In contrast, VEGFR2 in vehicle treated cells was uniformly distributed in small puncti throughout the cytoplasm. The VEGFR2 signal was clearly not associated with the ER marker PDI in either vehicle- or itraconazole-treated samples (Fig. 4*B*). Treatment with either castanospermine, dMM, or swainsonine failed to induce a similar VEGFR2 accumulation (Fig. 4*C*), suggesting

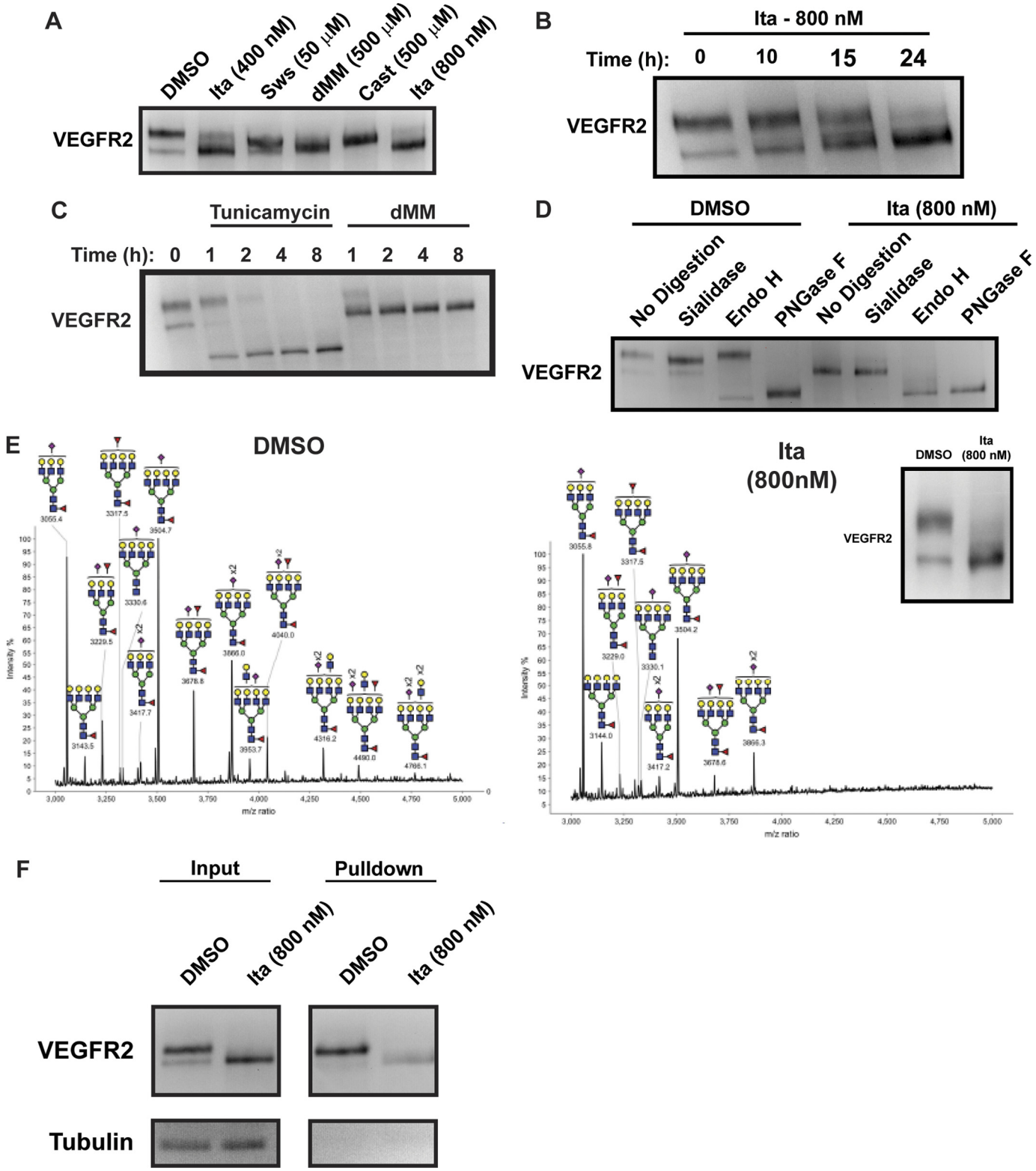

FIGURE 3. **Itraconazole alters *N*-linked glycosylation in HUVEC.** *A*, Western blot of VEGFR2 from HUVEC treated for 24 h with itraconazole (*Ita*) or *N*-linked glycosylation inhibitors Sws, dMM, or castanospermine (*Cast*). HUVEC were treated for the indicated times with 800 nM itraconazole (*B*), tunicamycin, or dMM (*C*) prior to analysis of VEGFR2 by Western blot. *D*, lysates from itraconazole- or vehicle-treated HUVEC were digested with sialidase, endo H, or PNGase F, and the migration pattern of VEGFR2 was analyzed by Western blot. *E*, partial MALDI-TOF mass spectra of the high molecular mass region of the global population of *N*-glycans from HUVEC treated with 800 nM itraconazole or vehicle alone. The *inset* shows a Western blot for VEGFR2 from samples of the cell pellets used for the global profiling. See supplemental Fig. 1 for complete spectra and a more detailed description of the annotations. *F*, cell surface proteins from itraconazole-treated HUVEC or vehicle controls were biotinylated, captured on streptavidin beads, and subjected to Western blotting. Tubulin, a control intracellular protein, was present only in the input fraction. *Yellow circles*, galactose; *green circles*, mannose; *blue squares*, *N*-acetylglucosamine; *yellow squares*, *N*-acetylgalactosamine; *red triangles*, fucose; *purple diamonds*, *N*-acetylneuraminic acid.

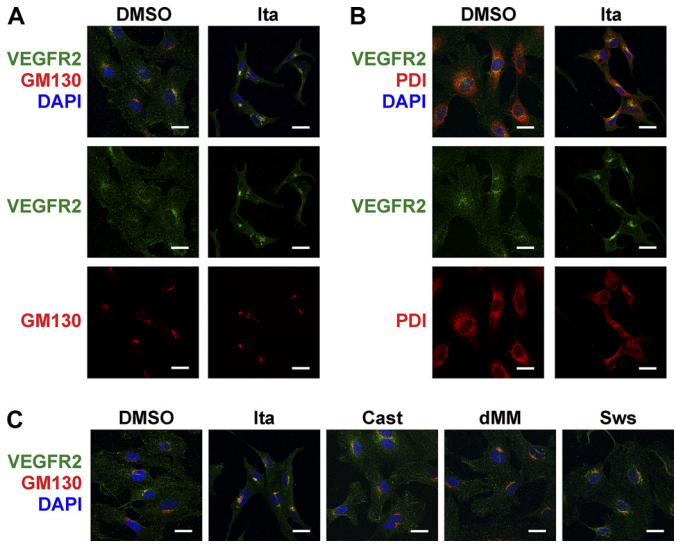

FIGURE 4. **Subcellular localization of VEGFR2 after treatment with itraconazole or other glycosylation inhibitors.** HUVEC were treated for 24 h with itraconazole (*Ita*; 800 nM) or vehicle (DMSO), fixed, and stained with anti-VEGFR2 and anti-GM130 (*A*), a *cis*-Golgi marker, or anti-PDI (*B*), an ER marker. *C*, cells were treated with 500 μM castanospermine (*Cast*), 500 μM dMM, 50 μM Sws, 800 nM itraconazole, or vehicle (DMSO) and treated as in *A*. Representative confocal micrographs are shown. *Bars*, 20 μm. Experiments were repeated in triplicate for GM130 staining experiments and in duplicate for PDI staining.

that the disruption in VEGFR2 trafficking seen after itraconazole treatment was probably not the result of impaired glycosylation.

N-Glycosylation is a complex process dependent on multiple enzymes that act sequentially on glycoproteins as they transit through the secretory system. To better understand at which stage itraconazole was arresting VEGFR2 processing, we characterized the *N*-glycan profile of itraconazole-treated HUVEC using MALDI-TOF mass spectrometry (Fig. 3*E* and supplemental Fig. 1). Itraconazole caused a clear reduction in high molecular weight tetra-antennary and poly-*N*-acetyllactosamine (poly-LacNAc)-containing *N*-glycans. This is demonstrated by the fact that the most abundant species in the depicted mass range after itraconazole treatment was a triantennary species at *m*/*z* 3055.8 compared with a tetra-antennary species at *m*/*z* 3504.7 without itraconazole treatment. Additionally, the poly-LacNAc-containing species at *m*/*z* 3953.7, 4316.2, 4490.0, and 4766.1 were no longer observed after itraconazole treatment. These differences would be associated with a deficiency in late *N*-glycan processing steps and in the case of the poly-LacNAc-containing *N*-glycans specifically with lack of processing by enzymes localized in the *trans*-Golgi compartment (37, 38). Notably, these mass spectroscopy data also indicated an increase in the relative abundance of $Man_5GlcNAc_2$ species, which is consistent with the effects of itraconazole in macrophages (11).

Itraconazole Inhibits the Glycosylation of EGFR in ACHN Cells and VEGFR1 in HUVEC—The results obtained from the global profiling of *N*-glycans from itraconazole-treated HUVEC suggested that the effects on glycosylation are not limited to VEGFR2. To validate this at the level of an individual protein, we examined a second isoform of VEGFR in HUVEC, VEGFR1, and found that itraconazole also affected its migration pattern with an effective concentration starting from 200 nM (Fig. 5*A*). This was similar to the concentration that induced hypoglycosylation of VEGFR2 and the IC_{50} for proliferation and the other itraconazole-induced phenotypes in HUVEC.

Next, we examined the effects of itraconazole on the *N*-glycosylation pattern of another RTK family member, EGFR, in ACHN cells, which is a renal carcinoma line. In an initial experiment, we determined whether itraconazole affected ACHN cell proliferation. Because itraconazole is highly protein-bound in serum, we reasoned that in this experiment, the potency of itraconazole would be serum concentration-dependent and therefore tested media with both 10 and 2% serum (Fig. 5*C*). As expected, ACHN cells were considerably more sensitive in 2% serum, with an EC_{50} of 373 nM. We note that even with 2% serum, ACHN cells were significantly less sensitive to itraconazole than HUVEC, as seen previously with other cell types (1). Because HUVEC are normally grown in 2% serum, we chose to use the 2% serum medium for the ACHN cell glycosylation experiments. Under these conditions, itraconazole increased the motility of EGFR starting near 500 nM, which is similar to the EC_{50} for ACHN cell proliferation, suggesting that the migration shift may be mechanistically linked to the effects on cell proliferation (Fig. 5*B*). Itraconazole also conferred endo H sensitivity to EGFR, indicating that, like VEGFR2 in HUVEC, itraconazole was able to modulate the *N*-glycosylation of EGFR in ACHN cells (Fig. 5*D*).

Glycosylation Inhibition Is Independent of Cholesterol Trafficking and mTOR Inhibition—We have previously reported that itraconazole has multiple effects on endothelial cells, including inhibition of cholesterol trafficking (NPC phenotype) and mTOR inhibition (9). The IC_{50} for HUVEC proliferation, cholesterol trafficking, mTOR inhibition, and VEGFR2 glycosylation were all similar, suggesting a common underlining mechanism. Thus, we sought to determine the relationship between VEGFR2 hypoglycosylation and these other activities of itraconazole. We first determined whether glycosylation inhibition in general could affect cholesterol trafficking by treating HUVEC with castanospermine, swainsonine, or dMM and imaging cholesterol localization with the cholesterol-binding dye, filipin (Fig. 6*A*). None of the glycosylation inhibitors was able to perturb cholesterol trafficking. Similarly, castanospermine, swainsonine, and dMM all failed to inhibit mTOR, as determined by the phosphorylation state of S6 kinase, a canonical mTOR substrate (Fig. 6*B*). We also tested whether direct blockade of cholesterol trafficking using U18666A or imipramine, known inducers of the NPC phenotype, or mTOR inhibition by rapamycin would lead to hypoglycosylation of VEGFR2 (Fig. 6*C*). None of these agents could recapitulate the effects caused by itraconazole.

Because itraconazole has pleiotropic effects, it was possible that an activity other than hypoglycosylation could be contributing to the inhibition of VEGFR2 signaling. Thus, we took advantage of small molecules that recapitulate subsets of itraconazole's activities to test their effects on VEGF-dependent activation of VEGFR2. Neither treatment with rapamycin, U18666A, nor dMM could mimic the effects of itraconazole on VEGR2 signaling (Fig. 6*D*). Thus, of the molecular activities associated with itraconazole, induction of hypoglycosylation

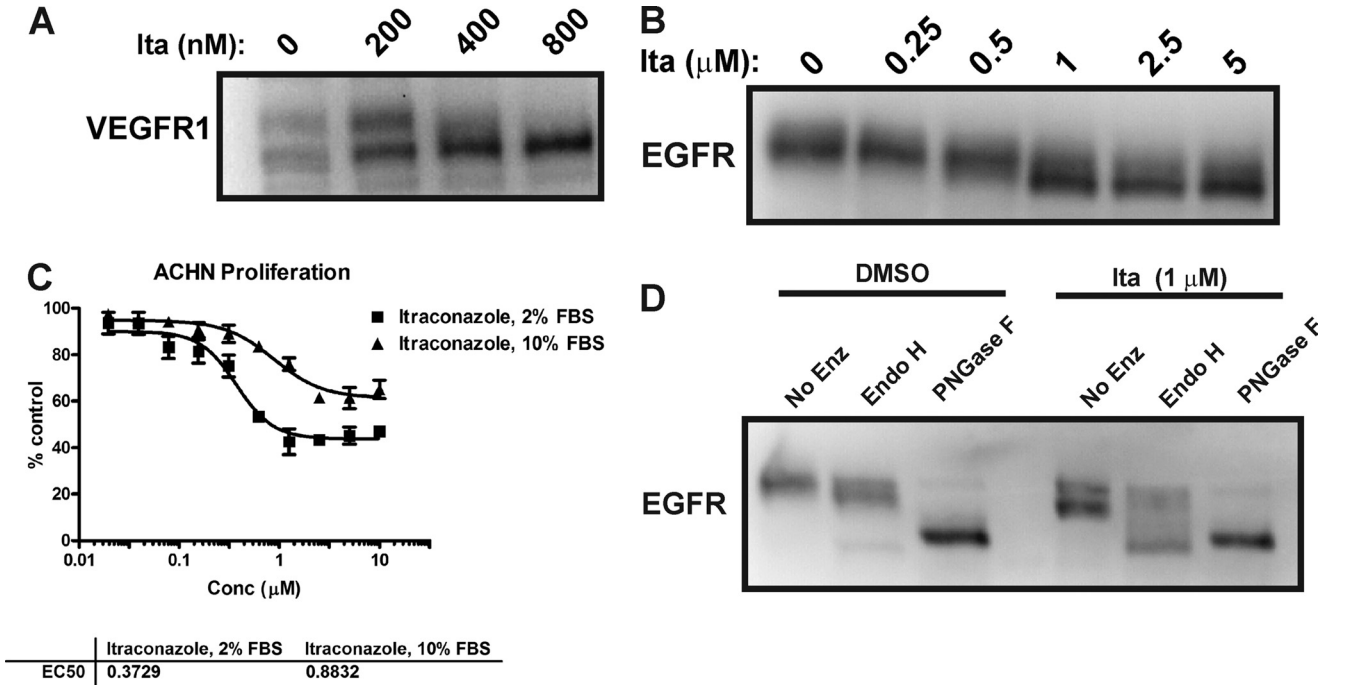

	Itraconazole, 2% FBS	Itraconazole, 10% FBS
EC50	0.3729	0.8832

FIGURE 5. **Itraconazole's effects on glycosylation extend beyond VEGFR2 and HUVEC.** *A*, HUVEC were treated with the indicated doses of itraconazole (*Ita*) or DMSO vehicle (0 μM itraconazole dose), and the migration pattern of VEGFR1 was analyzed by Western blot. *B*, ACHN cells were treated with the indicated concentrations of itraconazole in 2% serum, and EGFR was analyzed by Western blot. *C*, the effects of itraconazole on the proliferation of the renal cell carcinoma line, ACHN, in the presence of 2 or 10% serum. *D*, lysates from itraconazole-treated ACHN cells were digested with either endo H or PNGase F and analyzed by Western blot for EGFR. *Error bars*, S.E.

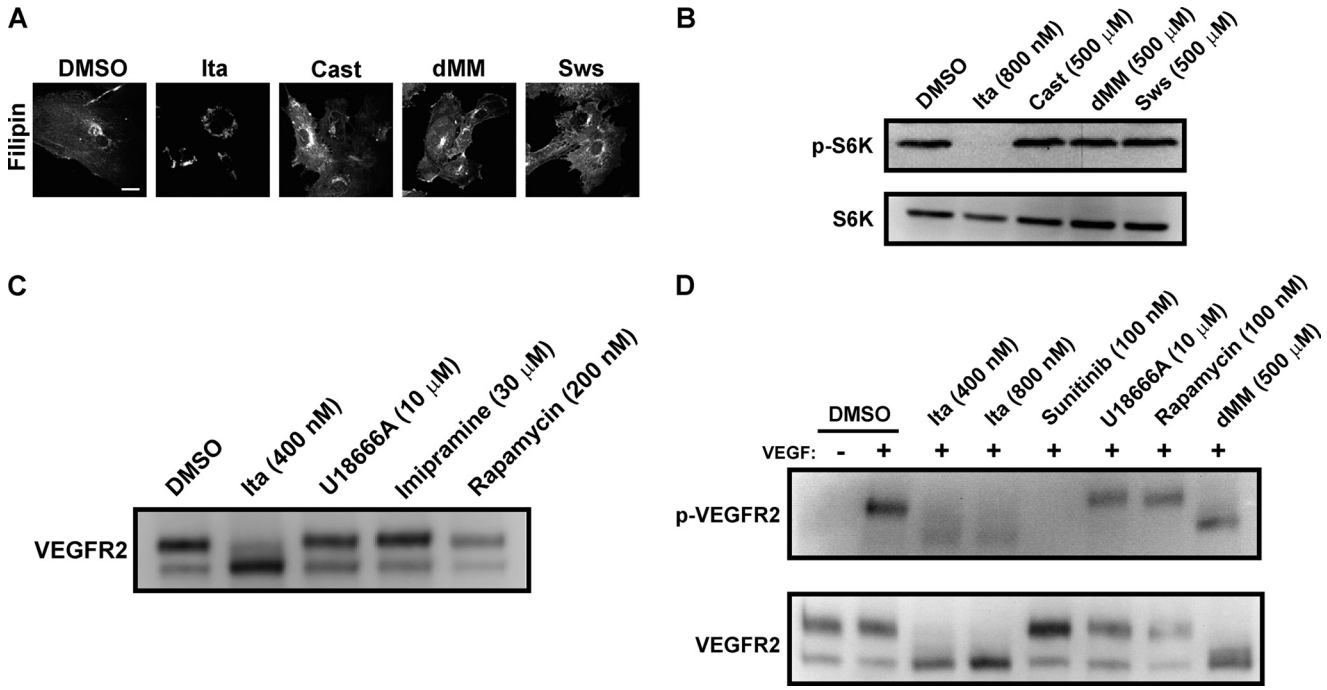

FIGURE 6. **Itraconazole's effects on VEGFR2 glycosylation occur in parallel to other itraconazole-induced effects.** *A*, cholesterol localization was visualized by filipin staining of HUVEC treated with 800 nM itraconazole (*Ita*), 500 μM castanospermine (*Cast*), 500 μM dMM, or 50 μM Sws. *Bar*, 20 μm. *B*, mTOR inhibition was determined based on the phosphorylation status of its substrate S6 kinase (*S6K*) after treatment with itraconazole, castanospermine, dMM, or Sws, as determined by Western blot. *C*, VEGFR2 migration patterns were analyzed by Western blot in lysates from HUVEC treated for 24 h with itraconazole, the mTOR inhibitor rapamycin, or two inhibitors of cholesterol trafficking, U18666A and imipramine. *D*, activation of VEGFR2 phosphorylation by $VEGF_{165}$ after treatment with the indicated compounds was assessed by Western blotting.

was the most closely linked to the inhibition of VEGF-induced VEGFR2 autophosphorylation. Interestingly, treatment with dMM did not block VEGFR2 activation, although dMM treatment also leads to hypoglycosylation.

Cholesterol Repletion Rescues Itraconazole-induced Glycosylation and VEGFR2 Signaling Inhibition—In earlier work, we found that the addition of cholesterol to HUVEC via a cyclodextrin carrier could rescue the effects of itraconazole on pro-

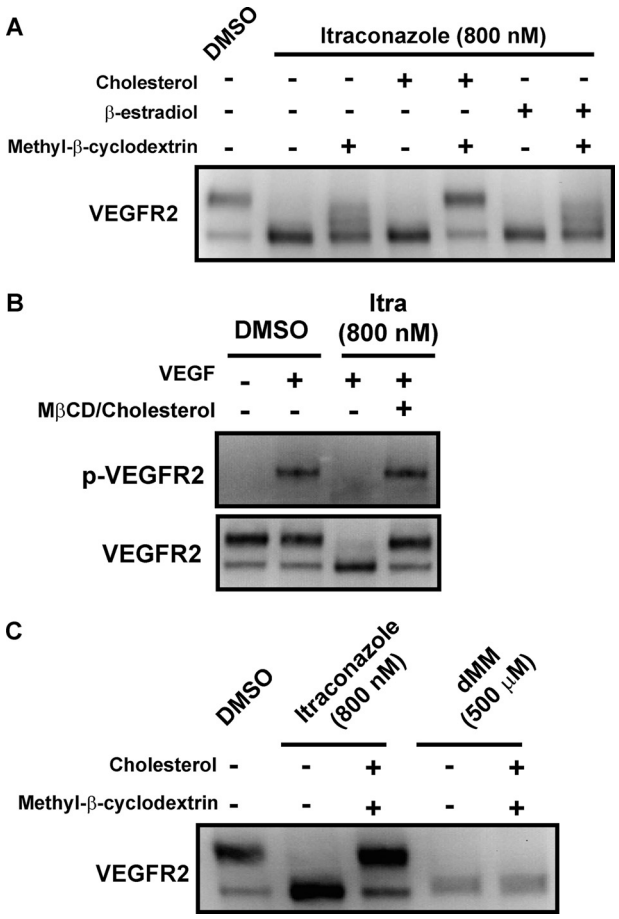

FIGURE 7. **Itraconazole-induced VEGFR2 hypoglycosylation and signaling inhibition is rescued by supplementation of cellular cholesterol.** *A*, HUVEC were treated with itraconazole or vehicle alone in the presence of free cholesterol or free β-estradiol, free methyl-β-cyclodextrin, methyl-β-cyclodextrin·cholesterol, or methyl-β-cyclodextrin·β-estradiol complexes. VEGFR2 migration patterns in lysates were analyzed by Western blot. *B*, the ability of methyl-β-cyclodextrin·cholesterol to rescue itraconazole (*Itra*)-induced VEGFR2 signaling inhibition in HUVEC after $VEGF_{165}$ stimulation was determined by Western blot. *C*, the capacity of methyl-β-cyclodextrin·cholesterol to rescue dMM-induced migration changes was determined as in *A*.

liferation and mTOR inhibition (9). This suggested that itraconazole-induced cholesterol mislocalization was the primary driver of itraconazole's global effects. However, given our new finding that cholesterol trafficking disruption by U18666A and imipramine could not induce VEGFR2 hypoglycosylation and that U18666A did not inhibit VEGF signaling, further exploration of the interplay between itraconazole's effects and cholesterol was warranted. We found that the addition of cholesterol via methyl-β-cyclodextrin·cholesterol complexes, but not methyl-β-cyclodextrin or free cholesterol alone, could rescue the itraconazole-induced hypoglycosylation of VEGFR2 and that methyl-β-cyclodextrin·cholesterol could also rescue itraconazole-induced VEGFR2 signaling inhibition (Fig. 7, *A* and *B*).

Importantly, the addition of methyl-β-cyclodextrin complexed with β-estradiol, a sterol related to cholesterol, had no effect on VEGFR2 glycosylation, suggesting that the cholesterol rescue was probably not a general effect of either a methyl-β-cyclodextrin·sterol complex or the total cellular sterol concentration (Fig. 7*A*). The methyl-β-cyclodextrin·cholesterol rescue of VEGFR2 was also specific to itraconazole-induced glycosylation changes because dMM-induced hypoglycosylation was not affected by cholesterol supplementation (Fig. 7*C*).

DISCUSSION

Because itraconazole was found to possess previously unknown antiangiogenic activity, it has been subject to extensive studies to deconvolute its mechanism of inhibition of endothelial cell proliferation and angiogenesis (1, 8, 9). Concurrently, it has entered multiple Phase II human clinical studies as a novel agent for treating cancer. Although itraconazole has been shown to inhibit mTOR and induce cholesterol trafficking defects in endothelial cells, how these activities relate to the overall effects in endothelial cells has remained unknown. In this work, we have identified a new mechanism by which itraconazole may be affecting angiogenesis. We have shown that itraconazole is capable of inducing VEGFR2 hypoglycosylation and that it strongly inhibits VEGFR2 autophosphorylation after VEGF stimulation. Blockade of VEGF binding, secondary to VEGFR2 trafficking defects, contributes to this mechanism. The effects of VEGFR2 signaling inhibition extend downstream to PLCγ1 activation. Consistent with studies in macrophages, the glycosylation effects we observed were not shared with other members of the azole class of antifungals or human 14DM inhibitors, thereby invoking a unique mechanism unrelated to 14DM inhibition (11). Notably, these effects occurred starting at 200 nM, which is far below itraconazole's steady state trough plasma level (2.6 μM) in patients on a standard 200-mg oral dosing regimen, suggesting that this mechanism may be relevant *in vivo* (SPORANOX® (itraconazole) package insert, PriCara, Raritan, NJ).

The serendipitous discovery of itraconazole's effects on VEGFR2 glycosylation and function makes itraconazole a unique antiangiogenic agent. It has been shown that inhibition of mTOR, cholesterol trafficking, or VEGFR signaling alone is sufficient to block endothelial cell proliferation and/or angiogenesis (9, 39). Because itraconazole is capable of simultaneously inhibiting mTOR and VEGFR2 signaling, its *in vivo* efficacy as an antiangiogenic agent may be significantly enhanced as a result. Interestingly, the blockade of VEGFR2 signaling after VEGF addition did not extend to the level of ERK1/2, suggesting that itraconazole may be affecting only a subset of VEGF-responsive receptors. Sunitinib, a direct inhibitor of multiple receptor tyrosine kinases, including VEGFR1, -2, and -3, PDGFRα, and PDGFRβ, blocked both PLCγ1 and ERK activation in our experiments (33). Thus, the activation of ERK1/2 by VEGF in the presence of itraconazole may be due to other VEGF-binding receptors or receptor complexes on HUVEC, suggesting that VEGFR2 may be preferentially sensitive to hypoglycosylation. Alternatively, the residual activation of VEGFR2 after itraconazole treatment may be sufficient to drive signaling via ERK1/2.

Having described a new activity of itraconazole in endothelial cells, we next determined the relationship between glycosylation inhibition and the known molecular effects of itraconazole. We found that the induction of cholesterol trafficking defects and mTOR inhibition occur in parallel to the hypogly-

cosylation effect, as evidenced by a lack of effect of mTOR and cholesterol trafficking inhibitors on VEGFR2 glycosylation and by a similar lack of effect of other glycosylation inhibitors on mTOR and cholesterol trafficking. This ruled out a causal relationship between those known activities of itraconazole and its effect on glycosylation. Intriguingly, all three activities are rescued by the addition of cholesterol in methyl-β-CD complexes, suggesting that each may be downstream of an as yet unidentified common target that is sensitive to subcellular cholesterol localization. The concentration of cholesterol differs between organelles and helps to mediate the function and organization of the membrane proteins that define organelle function (40). Thus, it is possible that modulation of cholesterol levels impacts glycosylation and mTOR function by altering the localization of integral membrane proteins that are either directly or indirectly essential for these processes.

In addition to assessing the effects of itraconazole on endothelial cells, we also tested the ability of itraconazole to alter glycosylation in a renal cell carcinoma line. In these cells, glycosylation of EGFR, another receptor tyrosine kinase, was inhibited at a potency that again correlated with the IC_{50} for proliferation. This is especially intriguing because itraconazole is currently involved in a clinical trial for non-small cell lung cancer, a subset of which is dependent on EGFR signaling (41). Itraconazole has also been reported to influence glycosylation of the CD14 receptor in macrophages (11). Although in these cases a functional consequence of hypoglycosylation has not been demonstrated, the findings do suggest that the effects of itraconazole on glycosylation may be cell type-independent. Because of this, glycosylation inhibition may play an important role in *in vivo* angiogenesis inhibition. Given the evidence we have presented that glycosylation is inhibited in both tumor cells and HUVEC, it is possible that in the tumor microenvironment, itraconazole may eventually be shown to block both tumor and endothelial cell growth factor signaling, thereby leading to additive or superadditive effects on the inhibition of tumor growth.

Our global analysis of *N*-linked sugars in itraconazole-treated HUVEC showed a widespread loss of poly-LacNAc and tetra-antennary complex *N*-glycans. The enzymes that synthesize poly-LacNAc are localized in the *trans*-Golgi network, suggesting that itraconazole may selectively affect *N*-glycan processing at the distal regions of the secretory pathway (37, 38). Because the hypoglycosylation of VEGFR2 appeared to occur distal to the calnexin/calreticulin chaperone system, it is difficult to explain the loss of cell surface VEGFR2 as a result of retention by calnexin/calreticulin in the ER. The coupling of a lack of *N*-glycan processing in the *trans*-Golgi and the decreased levels of VEGFR2 on the cell surface after itraconazole treatment suggests that VEGFR2 may be trapped in the Golgi. This model is supported by our finding of a Golgi-like VEGFR2 staining pattern after itraconazole treatment and a partial colocalization of VEGFR2 with the *cis*-Golgi marker, GM130. That the itraconazole-induced glycosylation effects on VEGFR2 occur up to 16 h more slowly than those induced by tunicamycin and dMM, which are direct inhibitors of glycosyltransferases, and that dMM does not inhibit VEGFR2 signaling implies that the itraconazole-induced glycosylation effects are probably secondary to a primary disruption of trafficking in the Golgi compartment.

An alternative but less likely model is that the exact structure of the sugars retained on VEGFR2 affects trafficking with sufficient specificity such that the sugar species retained after itraconazole treatment inhibits further trafficking, whereas those sugars retained after castanospermine, dMM, or swainsonine (Sws) treatment do not. In this case, a primary glycosylation defect would lead to a secondary inhibition of trafficking. Further exploration of the exact nature of the sugars retained on VEGFR2 would be useful in addressing this possibility. Importantly, in either model, the inhibition of VEGFR2 signaling is the result of a loss of cell surface expression.

A disruption of vesicular trafficking would also be consistent with the aggregate activities of itraconazole in HUVEC. For instance, lysosomal cholesterol levels can be modulated by mediators of trafficking, as observed by experiments in NPC fibroblasts in which lysosomal cholesterol is reduced by overexpressing Rab9 and Rab7, which promote retrograde trafficking from endosomes to the *trans*-Golgi, and from experiments in which dominant negative Rab7 and Rab9 interfered with the internalization of sphingolipid cargo, which also accumulates in NPC lysosomes (42, 43). Proper vesicular transport is also closely tied to glycosylation, as demonstrated by the case of Vsp74, a yeast protein that participates in Golgi retrograde transport and is required for the proper localization of glycosyltransferase enzymes (44, 45). Accordingly, *vsp74*Δ yeasts are unable to produce properly glycosylated proteins. The human homolog of Vsp74, GOLPH3, is an oncogene that regulates mTOR signaling, which we know is also disrupted by itraconazole (46). Thus, a defect in vesicular transport could potentially explain the cholesterol trafficking, mTOR, and glycosylation activities we have observed. Further unraveling the nature of the VEGR2 trafficking defect in HUVEC will likely yield useful insights into the mechanism of angiogenesis inhibition by itraconazole.

Acknowledgments—We thank Professor Gerald Hart, Prof. Carolyn Machamer, and members of the Liu laboratory for helpful discussions and advice. We are also grateful to Prof. Hans Hammers for the gift of ACHN cells, to Prof. Machamer for the gift of the GM130 antibody, and to Sarah Head for the careful reading of the manuscript.

REFERENCES

1. Chong, C. R., Xu, J., Lu, J., Bhat, S., Sullivan, D. J., Jr., and Liu, J. O. (2007) *ACS Chem. Biol.* **2,** 263–270
2. Aftab, B. T., Dobromilskaya, I., Liu, J. O., and Rudin, C. M. (2011) *Cancer Res.* **71,** 6764–6772
3. Folkman, J. (1971) *N. Engl. J. Med.* **285,** 1182–1186
4. Hurwitz, H., Fehrenbacher, L., Novotny, W., Cartwright, T., Hainsworth, J., Heim, W., Berlin, J., Baron, A., Griffing, S., Holmgren, E., Ferrara, N., Fyfe, G., Rogers, B., Ross, R., Kabbinavar, F. (2004) *N. Engl. J. Med.* **350,** 2335–2342
5. Sandler, A., Gray, R., Perry, M. C., Brahmer, J., Schiller, J. H., Dowlati, A., Lilenbaum, R., and Johnson, D. H. (2006) *N. Engl. J. Med.* **355,** 2542–2550
6. Hayes, D. F. (2011) *JAMA* **305,** 506–508
7. Ranpura, V., Hapani, S., and Wu, S. (2011) *JAMA* **305,** 487–494
8. Shi, W., Nacev, B. A., Bhat, S., and Liu, J. O. (2010) *ACS Med. Chem. Lett.* **1,** 155–159
9. Xu, J., Dang, Y., Ren, Y. R., and Liu, J. O. (2010) *Proc. Natl. Acad. Sci. U.S.A.*

107, 4764–4769
10. Kim, J., Tang, J. Y., Gong, R., Kim, J., Lee, J. J., Clemons, K. V., Chong, C. R., Chang, K. S., Fereshteh, M., Gardner, D., Reya, T., Liu, J. O., Epstein, E. H., Stevens, D. A., and Beachy, P. A. (2010) *Cancer Cell.* **17,** 388–399
11. Frey, T., and De Maio, A. (2009) *J. Biol. Chem.* **284,** 16882–16890
12. Nagy, J. A., Dvorak, A. M., and Dvorak, H. F. (2007) *Annu. Rev. Pathol.* **2,** 251–275
13. Cross, M. J., and Claesson-Welsh, L. (2001) *Trends Pharmacol. Sci.* **22,** 201–207
14. Ball, S. G., Shuttleworth, C. A., and Kielty, C. M. (2007) *J. Cell Biol.* **177,** 489–500
15. Ellis, L. M. (2006) *Mol. Cancer Ther.* **5,** 1099–1107
16. Kerbel, R. S. (2008) *N. Engl. J. Med.* **358,** 2039–2049
17. Rahimi, N. (2006) *Front. Biosci.* **11,** 818–829
18. Grünewald, F. S., Prota, A. E., Giese, A., and Ballmer-Hofer, K. (2010) *Biochim. Biophys. Acta* **1804,** 567–580
19. Nacev, B. A., Low, W. K., Huang, Z., Su, T. T., Su, Z., Alkuraya, H., Kasuga, D., Sun, W., Träger, M., Braun, M., Fischer, G., Zhang, K., and Liu, J. O. (2011) *J. Pharmacol. Exp. Ther.* **338,** 466–475
20. Neufeld, G., and Gospodarowicz, D. (1985) *J. Biol. Chem.* **260,** 13860–13868
21. Vaisman, N., Gospodarowicz, D., and Neufeld, G. (1990) *J. Biol. Chem.* **265,** 19461–19466
22. Jang-Lee, J., North, S. J., Sutton-Smith, M., Goldberg, D., Panico, M., Morris, H., Haslam, S., and Dell, A. (2006) *Methods Enzymol.* **415,** 59–86
23. Sutton-Smith, M., and Dell, A. (2006) in *Cell Biology: A Laboratory Handbook* (Celis, J. E., ed) pp. 415–425, Academic Press, Inc., San Diego, CA
24. Dell, A., Reason, A. J., Khoo, K. H., Panico, M., McDowell, R. A., and Morris, H. R. (1994) *Methods Enzymol.* **230,** 108–132
25. Ceroni, A., Maass, K., Geyer, H., Geyer, R., Dell, A., and Haslam, S. M. (2008) *J. Proteome Res.* **7,** 1650–1659
26. Christian, A. E., Haynes, M. P., Phillips, M. C., and Rothblat, G. H. (1997) *J. Lipid Res.* **38,** 2264–2272
27. Swinney, D. C., So, O. Y., Watson, D. M., Berry, P. W., Webb, A. S., Kertesz, D. J., Shelton, E. J., Burton, P. M., and Walker, K. A. (1994) *Biochemistry* **33,** 4702–4713
28. Lamb, D. C., Kelly, D. E., Waterman, M. R., Stromstedt, M., Rozman, D., and Kelly, S. L. (1999) *Yeast* **15,** 755–763
29. Trösken, E. R., Adamska, M., Arand, M., Zarn, J. A., Patten, C., Völkel, W., and Lutz, W. K. (2006) *Toxicology* **228,** 24–32
30. Takahashi, T., Yamaguchi, S., Chida, K., and Shibuya, M. (2001) *EMBO J.* **20,** 2768–2778
31. Takahashi, T., and Shibuya, M. (1997) *Oncogene* **14,** 2079–2089
32. Cunningham, S. A., Arrate, M. P., Brock, T. A., and Waxham, M. N. (1997) *Biochem. Biophys. Res. Commun.* **240,** 635–639
33. Faivre, S., Demetri, G., Sargent, W., and Raymond, E. (2007) *Nat. Rev. Drug Discov.* **6,** 734–745
34. Raymond, E., Dahan, L., Raoul, J. L., Bang, Y. J., Borbath, I., Lombard-Bohas, C., Valle, J., Metrakos, P., Smith, D., Vinik, A., Chen, J. S., Hörsch, D., Hammel, P., Wiedenmann, B., Van Cutsem, E., Patyna, S., Lu, D. R., Blanckmeister, C., Chao, R., and Ruszniewski, P. (2011) *N. Engl. J. Med.* **364,** 501–513
35. Ruch, C., Skiniotis, G., Steinmetz, M. O., Walz, T., and Ballmer-Hofer, K. (2007) *Nat. Struct. Mol. Biol.* **14,** 249–250
36. Helenius, A., and Aebi, M. (2004) *Annu. Rev. Biochem.* **73,** 1019–1049
37. Lee, P. L., Kohler, J. J., and Pfeffer, S. R. (2009) *Glycobiology* **19,** 655–664
38. Roth, J., and Berger, E. G. (1982) *J. Cell Biol.* **93,** 223–229
39. Yu, Y., and Sato, J. D. (1999) *J. Cell. Physiol.* **178,** 235–246
40. Lippincott-Schwartz, J., and Phair, R. D. (2010) *Annu. Rev. Biophys.* **39,** 559–578
41. Giaccone, G. (2005) *J. Clin. Oncol.* **23,** 3235–3242
42. Schweitzer, J. K., Krivda, J. P., and D'Souza-Schorey, C. (2009) *Curr. Drug Targets* **10,** 653–665
43. Choudhury, A., Dominguez, M., Puri, V., Sharma, D. K., Narita, K., Wheatley, C. L., Marks, D. L., and Pagano, R. E. (2002) *J. Clin. Invest.* **109,** 1541–1550
44. Schmitz, K. R., Liu, J., Li, S., Setty, T. G., Wood, C. S., Burd, C. G., and Ferguson, K. M. (2008) *Dev. Cell.* **14,** 523–534
45. Tu, L., Tai, W. C., Chen, L., and Banfield, D. K. (2008) *Science* **321,** 404–407
46. Scott, K. L., Kabbarah, O., Liang, M. C., Ivanova, E., Anagnostou, V., Wu, J., Dhakal, S., Wu, M., Chen, S., Feinberg, T., Huang, J., Saci, A., Widlund, H. R., Fisher, D. E., Xiao, Y., Rimm, D. L., Protopopov, A., Wong, K. K., and Chin, L. (2009) *Nature* **459,** 1085–1090